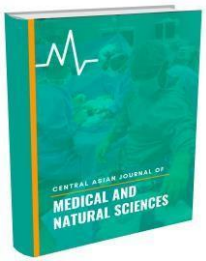

CENTRAL ASIAN JOURNAL OF MEDICAL AND NATURAL SCIENCES
https://cajmns.centralasianstudies.org/index.php/CAJMNS
Volume: 06 Issue: 01 | January 2025 ISSN: 2660-4159

Article

Cu3BiS3 Nanocomposites for Optoelectronics and NO2 gas Sensing

Hoolya Nadhim Nooruldeen[1], Mohanad Qader Kareem[2]

1,2. Department of Physics, College of Science, University of Kirkuk, Kirkuk, Iraq.
* Correspondence: scpm23009@uokirkuk.edu.iq.

Abstract: This paper focuses on Cu3BiS3 nanocomposites that were produced using solvothermal technique in the presence of a capping agent known as Mercaptoacetic acid (MMA). The study also shows that these nanostructures have the possibility of being used in optoelectronic and gas sensing industries. FE-SEM analysis, XRD diffraction pattern, and UV-Vis spectroscopy reveal regular nanostructures with crystalline nature and the ability to control their optical features. Electrical measurements show promising PIV performance and temperature-dependent Hall Effect measurements provide information about main charge transport channels. The study of the dynamic response of the nanocomposite to NO2 is performed through dynamic response curves as a function of operating temperature and shows a more detailed and richer interdependence between operating temperature and sensing performance. Interestingly, the sensitivity is maximized at 100°C which is a remarkable improvement in the development of the room-temperature gas detecting device. This work expands the knowledge on ternary chalcogenide nanocomposites and suggests ways in which they can be implemented in future optoelectronic and environmental applications. This systematic study helps in understanding the structural, optical, electrical and gas sensing characteristics of Cu3BiS3 nanocomposites for various technological applications.

Keywords: Cu3BiS3 nanocomposites; Optoelectronic materials; NO2 gas sensing; Nanostructured semiconductors; Chalcogenide-based sensors.

Citation: H. N. Nooruldeen, Mohanad Qader Kareem. Cu3BiS3 Nanocomposites for Optoelectronics and NO2 gas Sensing. Central Asian Journal of Medical and Natural Science 2025, 6(1), 376-391

Received: 15th Dec 2024
Revised: 26th Dec 2024
Accepted: 8th Jan 2025
Published: 21th Jan 2025

1. Introduction

The detection and monitoring of harmful gases have become increasingly critical in modern society, driven by growing concerns about air quality, industrial safety, and environmental protection[1].The development of highly sensitive, selective, and cost-effective gas sensors plays a vital role in addressing these challenges, finding applications in diverse fields such as environmental monitoring, industrial process control, and public health [2].In recent years, the quest for improved gas sensing technologies has led researchers to explore novel materials and nanostructures, aiming to overcome the limitations of traditional sensing platforms[3]. Among the various materials being investigated for next-generation gas sensors, metal chalcogenide nanocomposites have emerged as promising candidates due to their tunable properties and high surface-to-volume ratios [4].These materials offer unique advantages in terms of sensitivity, selectivity, and response times, making them particularly attractive for gas sensing

applications [5].The possibility to control electronic and surface states of the metal chalcogenides by the proper synthesis and functionalization allows developing highly sensitive gas sensing materials. Ternary chalcogenide Cu3BiS3 semiconductor has attracted growing research interests in the last few years for its uses in photovoltaic, and sensor devices[6] . It has been found that the suitable bandgap of this material is approximately in the range of 1. 2-1. 4 eV and its high absorption coefficient makes it suitable for numerous optoelectronic applications.The complex crystal structure of Cu3BiS3as well as its inherent p-doping features make it possible to develop new type of sensing mechanisms and improve the performance of the Cu3BiS3-based sensors [7]. Incorporation of capping agents like mercaptoacetic acid during the synthesis of Cu3BiS3nanocomposites provides a fair chance to modify the characteristics of the material for application at gas sensing. Across these categories, capping agents have a key function in regulating particle size, avoiding agglomeration, and altering surface chemistry, all of which are essential aspects that define the gas sensing efficiency of the nanostructured materials[5]. The choice and the optimization of the capping agent in the synthesis allows manipulating the electronic and surface properties of Cu3BiS3 nanocomposites and thus enhancing the gas sensing parameters such as sensor sensitivity, selectivity and stability. The advancements in preparation of nanomaterial and fabrication of sensing devices has empowered the researchers to design more sensitive and selective gas sensors[8]. The usage of nanostructures like the Cu3BiS3 in the development of sensors have also indicated that it can enhance sensitivity and response time of the sensing devices.The nanostructured materials are characterised by a high surface to volume ratio that means that there are many active sites at which gas adsorption and reaction can take place, thus increasing the overall performance of sensors [9]. Also, the changes in the electronic structure due to the interference of the nanomaterials can lead to higher changes in electrical conductivity for exposure to the target gases and thus, trace level detection.Based on the well-established body of knowledge on metal oxide and chalcogenide-based sensors, Cu3BiS3 nanocomposites have been implemented in gas sensing. The initial metal oxide sensors, SnO2, ZnO, and WO3 have been extensively explored, and their applications are relatively well-established[10] . Unfortunately, these materials are known to have some drawbacks among which are high operating temperature, nonselective, and humidity sensitivity .These challenges can be met with Cu3BiS3 nanocomposites since those materials combine qualities of ternary chalcogenides and a nanostructure approach .Nevertheless, Cu3BiS3 material possess p-type semiconducting nature which will be highly preferable for the gas sensing application[11]. Unlike n-type semiconducting material that is widely used in metal oxide gas sensors, p-type materials respond differently and may have different sensing modes to specific gases[12].This characteristic enables designing new complementary sensing devices and feasible enhancement of existing ones selectivity through the design of p- n junction based sensors. Self-organized Cu3BiS3 nanowires were synthesized on Cu foil and on a Cu grid for TEM and STEM investigations .The synthesis of nanocomposites can be done through several approaches with each approach having some benefits in in terms of particle size, particle shapes and chemical compositions regulation [13]. Common preparation techniques include hydrothermal/solvothermal synthesis, hot-injection methods as well as chemical bath deposition including deposition, mechanochemical synthesis, and the microwave assisted synthesis. The as can be clearly seen, the selection of the synthesis method can significantly affect the characteristics of the structures, such as the crystal structure, the number of defects and the surface of nanocomposites.characteristics . By the introduction of mercaptoacetic acid into the synthesis House as a capping agent adds one more level of the control to the desired properties of the nanocomposite. Mercaptoacetic acid may adsorb at the surface of growing nanoparticles and thus restrain their size and possibility of further agglomeration . This surface modification can also change the electronic properties of the base ion of In fact, Zhou et al. established that the state of

nanoparticles can be altered so that it can improve its interaction with the target gas molecules. In addition, PVP likely adsorbs directly on the NASQ cluster because the functional groups from the capping agent were detected on the nanoparticle. interface can create a large number of new active sites for the adsorption of gas or catalytic reaction, it may relative enhancement in achieving overall sensing performance . The structure, properties and the gas sensing mechanism of Cu3BiS3 nanocomposites, the sensing mechanism is founded on alterations in the electrical conductivity if the material in response to target gases . In the case of p-type semiconductors such as Cu3BiS3, interaction with oxidizing gas lead to an oxidation of[14]

An increase in the number raises the conductivity level and the reduction of gases lowers the conductivity. The exact sensing The working mechanism of the active layer can as well be complicated, which includes processes such as surface adsorption, charge transfer processes and so on interfacial reactions of the nanoparticle. Understanding these mechanisms is necessary in fine tuning the sensors and formulating ways of improving the sensitivity of the sensors and selectivity. The purpose of this work is to reveal the possibility of using Cu3BiS3 for gas sensing applications with Studies were conducted on the synthesized Fe3O4-loaded mercaptoacetic acid nanocomposites, with a view of assessing the structural stability and sensitivity of the nanocomposites on exposure to NO2 at various operating temperatures. NO2 is one of the most widely spread air pollutants and it has been In relation to the combustion processes and has huge effects on the overall human health and environmental quality. Low concentration monitoring of NO2 emissions is therefore important as indicated by the results above.safety monitoring in industries and other related quality control and assurance properties[15].By investigating the relationship between material properties and sensing performance, we seek to contribute to the ongoing development of next-generation gas sensors for environmental monitoring and safety applications. Specifically, this research aims to address the following objectives:Specifically, this research aims to address the following objectives :

i. Synthesis and characterization of Cu3BiS3 nanocomposites with tunable morphology and composition with the help of mercaptoacetic acid as a capping agent.

ii. Examine the effects of synthesis parameters and post-synthesis treatments for the physical and chemical characteristic of the nanocomposites.

iii. Assess the gas sensing response of Cu3BiS3 (mercaptoacetic acid) nanocomposites for NO2 with varying operating temperatures.

iv. Examine the influence of nanocomposite properties such as size of the particles, surface area, defect density on gas sensing properties of nanocomposites such as sensitivity, response time and selectivity

v. Consider the ways to increase selectivity and stability by modifying the surface of the sensor or by forming organic/inorganic composites.

The subsequent Sections will present the literature review of the development of gas sensors, explore the processes of preparedness of Cu3BiS3 nanocomposites, and describe the properties of Cu3BiS3 nanocomposites to be used for gas sensing. Moreover, the other potential practical uses of Cu3BiS3 nanocomposites will be also discussed and further research on this subject will be described because this is a dynamically developing branch of knowledge. This work is expected to extend our knowledge on Cu3BiS3 (mercaptoacetic acid) nanocomposites and the utilization of those nanocomposites in designing better, selective, and sensitive gas sensors. Such advancements are useful in gas detection in areas such as environmental monitoring, industrial safety and health through improving on the speed and precision of detecting dangerous gases.

2. Materials and Methods

The Cu3BiS3 nanocomposite was synthesized using the following precursors:

Bismuth nitrate (Bi(NO3)3·5H2O): 0.97 g (2 mmol) , Copper chloride (CuCl): 0.59 g (6 mmol) , Thiourea (CH4N2S): 0.46 g (6 mmol), Polyvinylpyrrolidone (PVP, MW ≈ 40,000): 1.0 g , Mercaptoacetic acid (C2H4O2S): 0.35 mL (5 mmol) .

2.2.Synthesis Procedure of Cu3BiS3 (Mercaptoacetic acid)

Cu3BiS3 (Mercaptoacetic acid) nanocomposite a was prepared using the Solvothermal synthesis method as it enables fine control over the size and shape of the nanomaterials as illustrated by figure 1.

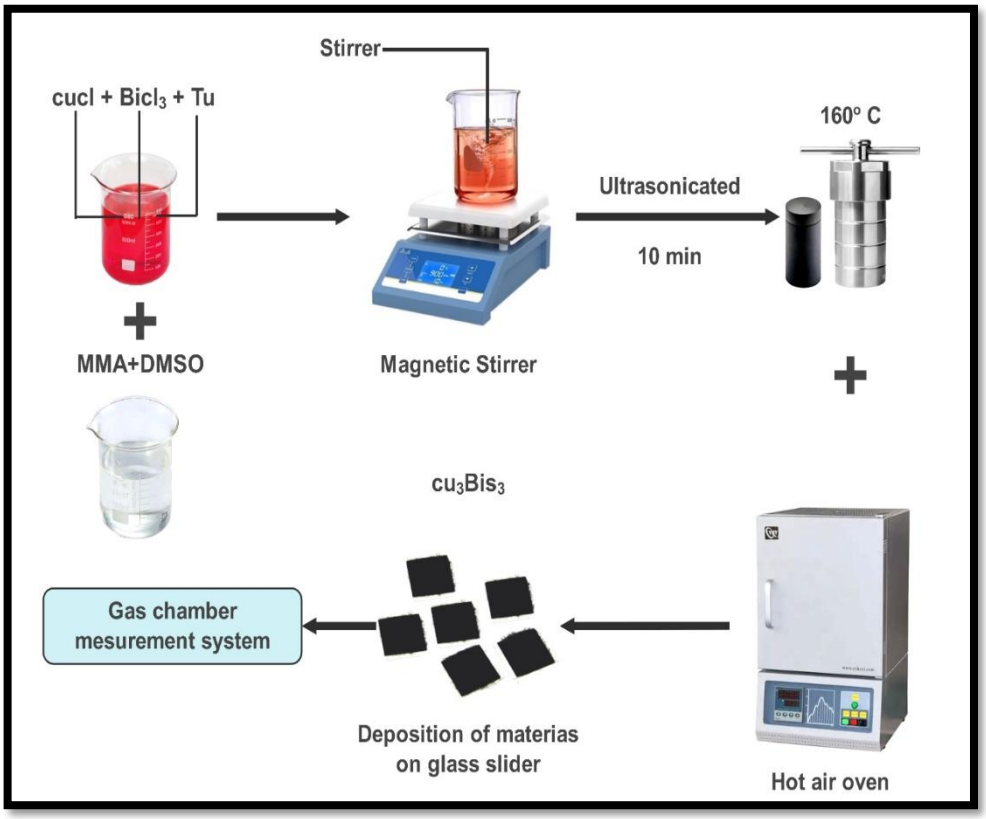

Figure 1. Schematic for the synthesis of Cu3BiS3 (Mercaptoacetic acid) nanocomposite.

The procedure was as follows: Bismuth nitrate (0. 97 g, 2 mmol) was dissolve in 20 mL of dimethyl sulfoxate (DMSO) in a 100 mL round bottom flask with the help of magnetic stirrer.. DMSO was chosen as the solvent due to its high boiling point and ability to dissolve metal salts effectively .

Copper chloride (0.59 g, 6 mmol) was added to the solution and stirred until completely dissolved. The 3:1 molar ratio of Cu to Bi was maintained to ensure the formation of the desired Cu3BiS3 stoichiometry. Thiourea (0.46 g, 6 mmol) was introduced as the sulfur source, followed by thioglycolic acid (0.28 mL, 4 mmol). Thiourea provides a controlled release of sulfur ions during the reaction, while thioglycolic acid acts as a complexing agent to regulate the release of metal ions. Polyvinylpyrrolidone (1.0 g) was added as a stabilizing agent. PVP helps prevent agglomeration of nanoparticles and contributes to size control. The solution was stirred for 30 minutes to ensure homogeneous mixing. Mercaptoacetic acid (0.35 mL, 5 mmol) was slowly added to the mixture while stirring. This compound serves as a capping agent, controlling nanoparticle growth and morphology by binding to the surface of growing crystallites. The resulting solution was transferred to a 50 mL Teflon-lined stainless steel autoclave. The use of an autoclave allows for the generation of high pressure and temperature conditions necessary for the solvothermal reaction. The sealed autoclave was heated in an oven at 180°C for 24 hours. This extended reaction time ensures complete formation of the Cu3BiS3 phase and allows

for crystal growth. After the reaction, the autoclave was allowed to cool naturally to room temperature to prevent thermal shock and ensure uniform particle formation. The precipitate was collected by centrifugation at 4000 rpm for 10 minutes. This speed and duration were optimized to ensure complete separation of the nanoparticles from the reaction medium. The product was washed three times with deionized water and twice with absolute ethanol to remove unreacted precursors and byproducts. This thorough washing process is crucial for obtaining high-purity nanocomposites. The final Cu3BiS3 (Mercaptoacetic acid) nanocomposite was dried in a vacuum oven at 60°C for 12 hours to remove any residual solvents

2.3. Post-Synthesis Processing

To prepare the nanocomposite for further characterization and application:The dried black compound powder was ground in an agate mortar to ensure uniform particle size distribution. The powder was dispersed in 20 mL of ethanol and filtered through a 0.22 μm syringe filter to remove any large aggregates.Glass substrates were cleaned with acetone, ethanol, and deionized water successively to ensure a clean surface for deposition.Using an insulin needle, 100 μL of the filtered suspension was applied onto the glass substrate at 100°C. This elevated temperature promotes rapid solvent evaporation and improves film uniformity.The droplet was allowed to spread and dry at room temperature for 30 minutes. This process was repeated 2-3 times to achieve the desired thickness.The dried product was transferred to a muffle furnace and calcined at 300°C for 3 minutes to obtain the target product. This brief high-temperature treatment helps improve crystallinity and remove any remaining organic residues.

2.4. Characterization Techniques

The synthesized Cu3BiS3 (Mercaptoacetic acid) nanocomposite was thoroughly characterized using the following techniques: X-ray Diffraction (XRD): An Advance D8 diffractometer (Bruker Co., Ltd., Germany) was used with CuKα1 radiation (λ = 0.15406 nm) at 30 kV and 40 mA. The scanning rate was 2° per minute in the 2θ range of 10 to 80. From XRD spectra, one can obtain knowledge about crystal structure, phase purity and size of crystallites.Field Emission Scanning Electron Microscopy (FE-SEM): In the present work, a TESCAN MIRA3/RAITH LIS from France was used at an accelerating voltage of 5 kV to study the morphology and nanostructures of the product. Several advantages associated with FE-SEM include: high resolution imaging on the surface features as well as particle shapes. Energy Dispersive X-ray Spectroscopy (EDX): High-resolution imaging was utilised with the FE-SEM attachment for elemental composition identification giving details on the stoichiometry and the purity of the nanocomposite. UV-Visible Spectroscopy: For absorbance spectra of UV part, a Shimadzu spectrophotometer was applied. This analysis allows one to define the optical properties and predict the value of the Bandgap of the material which is important for work in the field of optoelectronics. Hall Effect measurements: These were carried out to ascertain electrical transport characteristics including carrier density, carrier mobility and conductivity. To this end, these parameters are crucial when assessing the material's suitability to electronic and sensing applications. IV Measurements: Dark and illuminated I -V characteristics of the nanocomposite. Gas Sensing Measurements: The sensing properties of the fabricated Cu3BiS3 (Mercaptoacetic acid) nano-composite were investigated based on the home-designed gas sensor setup. The sensor was fabricated by spin coating the nanocomposite on to inter-digitized electrodes on an alumina substrate. Variations in the electrical resistance of the sensor with respect to different quantities of NO2 gas at various operational temperatures (room temperature, 1000C and 2000C) were evaluated using this prepared gas sensor. Hence this review intends to investigate the structural, optical, electrical, and GAS sensing properties of Cu3BiS3 (Caprylic acid) nanocomposite for their potential application in optoelectronic devices and environmental analysis which is a topic less explored.

3. Results

3.1. Morphological and Compositional Analysis of Cu3BiS3 Nanocomposites via FE-SEM and EDX

The provided figure 2 Summarize the characterization of Cu3BiS3 nanocomposite synthesized using Mercaptoacetic acid as the capping agent. These are FE-SEM low magnification images and high magnification images; and EDX spectroscopy. Two micrographs in Figures 2A and 2B are FE-SEM micrographs at 35,000x and 70,000 x of magnification, respectively.

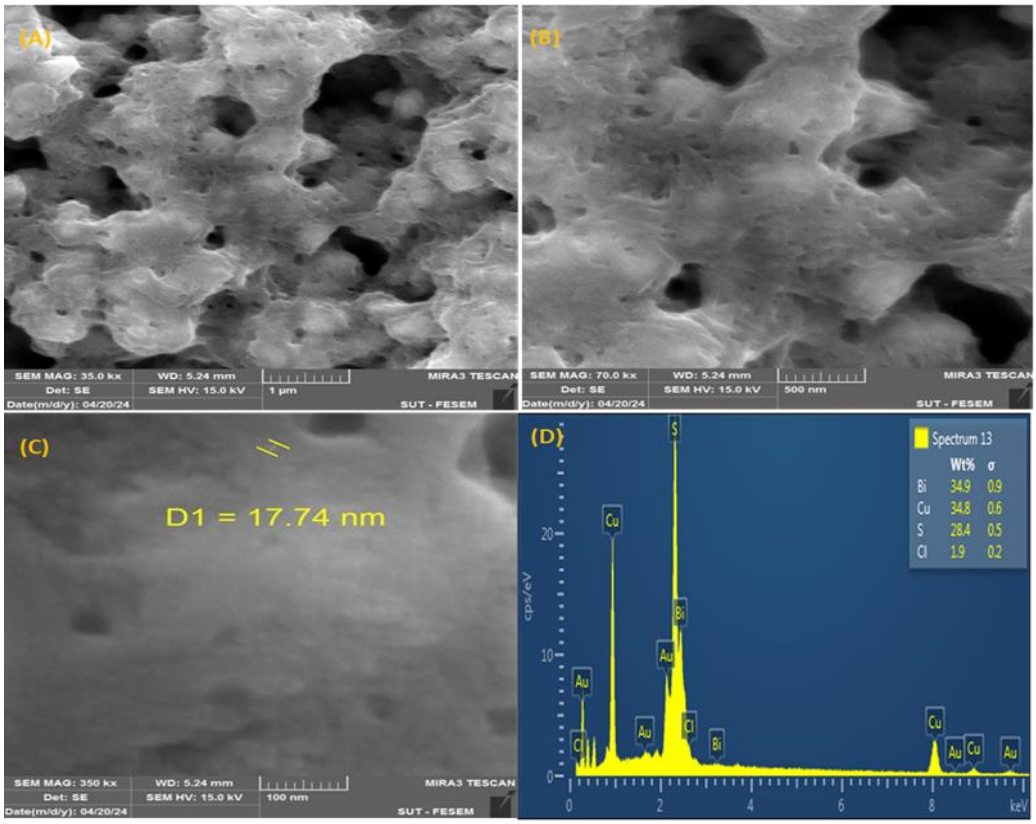

Figure 2 . FE-SEM micrographs of Cu3BiS3 (Mercaptoacetic acid) nanocomposite: FE-SEM Imaging, EDX Analysis at magnification : (A) 35kx , (B) 70.0kx , (C) 350kx, and (D) EDX analysis of films.

These images explain the fact that the nanocomposite has a porous, sponge-like structure with large surface area. The structure profile shows inter-connected particles that have many voids, which implies a high surface area. This morphology could be advantageous for applications requiring extensive surface interactions, such as catalysis or sensing. Figure 2C presents a higher magnification (350,000x) FE-SEM image, where a specific nanostructure is measured. The annotation indicates a dimension (D2) of 17.74 nm, which likely represents the size of an individual nanoparticle or a structural feature within the composite. This nanoscale dimension confirms the successful synthesis of nanoscale materials. The EDX spectrum in Figure 2D provides elemental composition data for the nanocomposite. The spectrum shows prominent peaks for copper (Cu), bismuth (Bi), and sulfur (S), corroborating the intended Cu3BiS3 composition. The quantitative analysis on the right side of the spectrum gives the weight percentages of the constituent elements: Sulfur (S): 34.9%, Copper (Cu): 34.8%, Bismuth (Bi): 28.4%, Chlorine (Cl): 1.9%. The presence of chlorine, albeit in a small quantity, may be attributed to residual precursors or solvents used during synthesis. The atomic concentrations of Cu, Bi, and S are close to the stoichiometric values of 3:1:3 of Cu:Bi:S as predicted for the Cu3BiS3 target material, thus suggesting successful formation of the material. These characterization results yield a detailed understanding of the nanocomposite's structural and compositional features of Cu3BiS3. The fact that this material has a high porosity and its main features have a nanoscale also indicates possible uses in areas where the benefits outweigh the drawbacks

of a large surface area and quantum confinement. , future works can be made to determine the full optical, electrical, as well as the catalytic properties of this material concerning its versatility in different technologies.

3.2. Crystalline Structure Determination of Cu3BiS3 Nanocomposites through XRD Patterns.

The XRD analysis illustrated in Figure 3 provides key insights into the nanocomposites crystal structure and phase purity. The upper panel exhibits the experimental diffraction pattern, characterized by well-defined, sharp peaks indicative of a highly ordered material with minimal defects. The lower panel displays the reference pattern (JCPDS 00-009-0488) facilitating direct comparison and definitive phase identification. The experimental pattern exhibits intense peaks aligning with the (111), (220), and (122) lattice planes, signatures of the intricate Cu3BiS3 crystal structure. Less prominent yet still discernible peaks including the (011), (321), and (133) further corroborate the development of the complex, long-range ordered Cu3BiS3 atomic lattice. The defined nature of these reflections indicates excellent crystallinity on an atomic scale.

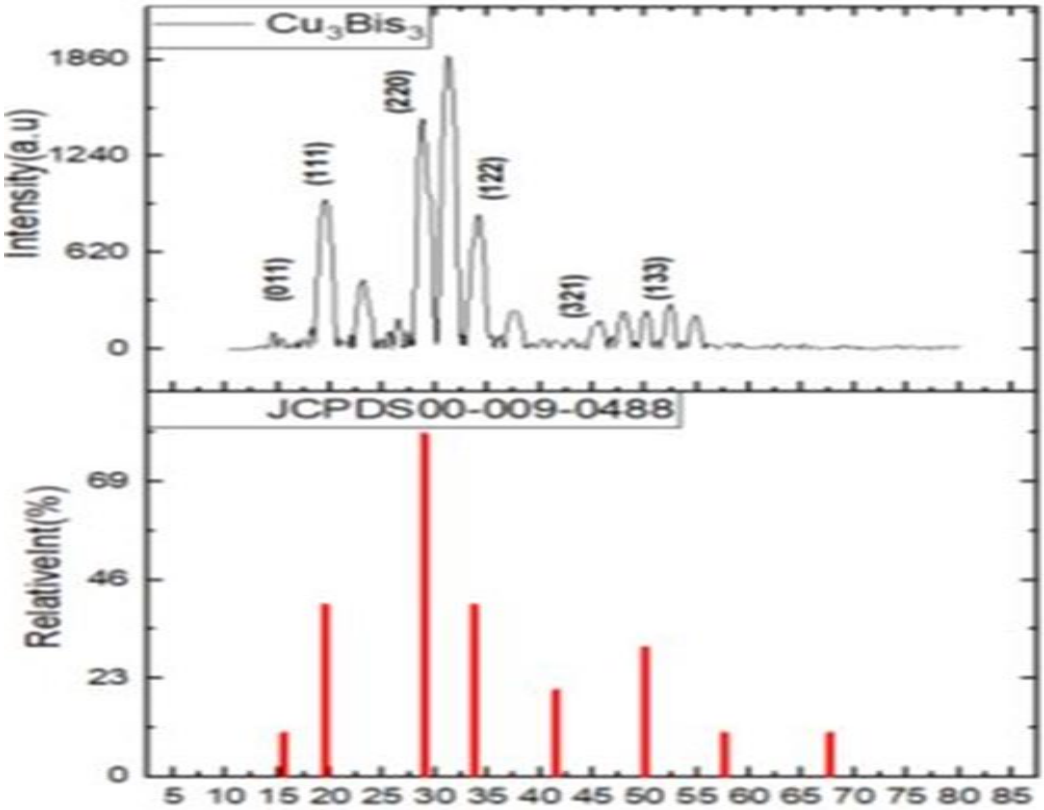

Figure 3. XRD patterns , and Grid profile of Cu3BiS3 (Mercaptoacetic acid) nanocomposite.

Meanwhile, their relative intensities provide information about preferential orientations for crystal growth along specific crystallographic directions.. A detailed analysis of the diffraction data is presented in Table 1, which compares the experimental results with the reference data. The table includes information on the 2θ positions, full width at half maximum (FWHM) values, d-spacing, and Miller indices (hkl) for the most significant peaks. The close agreement between the experimental d-spacing and those from the JCPDS reference card confirms the formation of the orthorhombic Cu3BiS3 phase. The slight variations in d-spacing, represented as percentage contractions in Table 1, may be attributed to strain effects in the nanocrystalline material. These minor deviations are consistent with the nanoscale nature of the synthesized composite, as evidenced by the peak broadening observed in the experimental pattern.

Table 1: Lattice distance (hkl) estimated by XRD, JCPDS, information card for identically (hkl) levels percentile variance of d and FWHM values for Cu3BiS3 (Mercaptoacetic acid) nanocomposite.

2θ (deg)	FWHM =β(Deg)	d(xrd) (⁰A)	D(JCPDS) (⁰A)	% Contraction in d	hkl	Phase	Card No
15.589	0.3936	5.62087	5.68000	0.05913	011	Orthorhombic	00-009-0488
19.494	0.2952	4.53119	4.55000	0.01881	111	Orthorhombic	00-009-0488
28.967	0.3444	3.08010	3.08000	-0.0001	220	Orthorhombic	00-009-0488
33.666	0.3444	2.64348	2.66000	0.01652	122	Orthorhombic	00-009-0488
41.584	0.5904	2.17581	2.17000	-0.00581	321	Orthorhombic	00-009-0488
50.049	0.1467	1.82301	1.82100	-0.00201	133	Orthorhombic	00-009-0488

The FWHM values, ranging from 0.2952° to 0.5904°, provide quantitative data on this broadening, which can be used to estimate crystallite sizes using the Scherrer equation. Of particular interest is the (220) reflection at 28.967°, which shows a perfect match in d-spacing with the reference data, indicating that this plane is minimally affected by strain. Conversely, the (011) plane exhibits the largest contraction (0.05913%), suggesting anisotropic strain within the crystal structure. The intricate XRD analysis, probing the material's inner workings on an atomic scale, validated the phase purity of the synthesized Cu3BiS3. The pattern emerged without a trace of spurious diffraction lines, showing that there were no impurities. That homogeneity is important for reliable performance and consistent behavior, which are critical for downstream applications in fields ranging from photovoltaics to thermoelectrics.

4. Discussion

The complementary characterization techniques including the informative SEM observation as well as distinctive EDX mapping converged to providing a well-rounded image of the material's microscopic nature. In this context, uncovering the structural details from such a comprehensive investigation is essential for correlating with property etymology and tailoring synthesis towards various technological applications. It usually takes a combination of tools to properly illuminate this black box of advanced materials so that we can make new advancements from it. the broadening due to small crystallite size may be expressed as [16]:

$$\beta = \frac{k\lambda}{t\cos\theta} \quad (1)$$

3.3. Optical Properties and Bandgap Engineering of Cu3BiS3 Nanocomposites.

Figure 4 reveals a detailed optically characterization of the Cu3BiS3 nanocomposite, prepared using Mercaptoacetic acid as capping agent. These consist of three plots (A, B and C) that provide key information on the material's optical properties and electronic band structure.

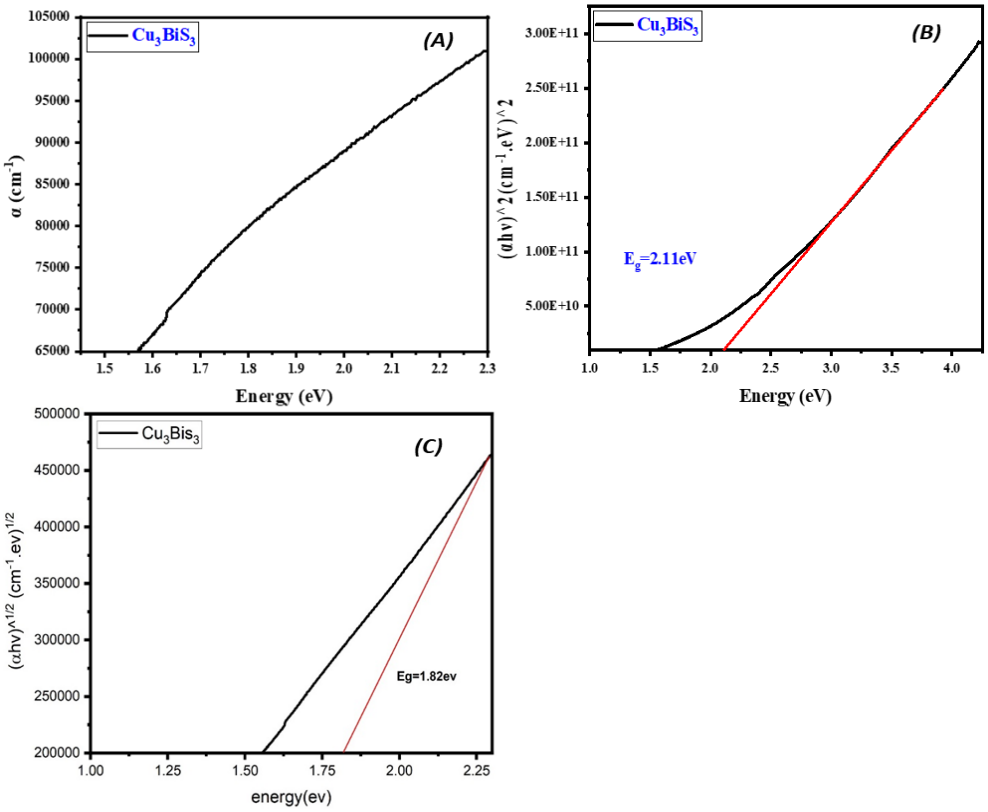

Figure 4. Optical band gap energy of a set of plots showing relationships between wavelength, absorbance, energy, and various derived quantities for Cu3BiS3 (Mercaptoacetic acid) nanocomposite.

plot A: the absorption coefficient (α) as a function of photon energy The absorption coefficient steadily grows with increasing photon energy, displaying a sharp surge around 1.6 eV. This behavior is telling of a semiconductor material, where the initiation of strong absorption corresponds to the stimulation of electrons across the bandgap. The gradual increase in absorption at lower energies may be attributed to sub-bandgap transitions, potentially because of defect states or band tailing effects common in nanostructured materials. Plot B illustrates the Tauc plot for the Cu3BiS3 nanocomposite, where (αhν)2 is plotted against photon energy (hν). This representation is employed to pinpoint the optical bandgap of direct bandgap semiconductors. The linear section of the curve is extrapolated to the x-axis, yielding a bandgap energy (Eg) of 2.11 eV. This value is significantly higher than the bulk Cu3BiS3 bandgap (typically around 1.4 eV), signifying quantum confinement effects due to the nanoscale dimensions of the material. The wider bandgap could potentially enhance the material's performance in optoelectronic applications, particularly in visible light absorption for photovoltaic devices. Plot C presents an alternative method for bandgap determination, showing (αhν)1/2 versus photon energy. This plot is typically used for indirect bandgap semiconductors. The extrapolation of the linear region to the x-axis in this case yields a bandgap of 1.82 eV. The discrepancy between the bandgap values obtained from plots B and C (2.11 eV vs. 1.82 eV) warrants further investigation. It could indicate the presence of both direct and indirect transitions in the material, or it might suggest that the nanocomposite exhibits characteristics of both direct and indirect bandgap semiconductors due to its nanostructured nature. The observed optical properties of the Cu3BiS3 nanocomposite have several implications:

1) The tunable bandgap in the visible range makes this material potentially suitable for solar cell applications, particularly in tandem or multi-junction devices,

2) The higher bandgap compared to bulk Cu3BiS3 could lead to improved open-circuit voltage in photovoltaic devices, potentially enhancing overall efficiency,

3) The presence of sub-bandgap absorption might indicate

the existence of intermediate energy levels, which could be exploited in photocatalysis or hot carrier collection in advanced solar cell designs, and

4) The apparent dual nature of the bandgap (direct and indirect) could offer unique opportunities in optoelectronic applications, potentially combining the high absorption coefficient of direct bandgap materials with the longer carrier lifetime characteristic of indirect bandgap semiconductors.

Further studies, such as temperature-dependent optical measurements and photoluminescence spectroscopy, would be valuable in elucidating the exact nature of the electronic transitions and quantifying the influence of quantum confinement effects on the optical properties of this Cu3BiS3 nanocomposite. Additionally, correlating these optical characteristics with the material's structural properties, as revealed by XRD and SEM analyses, could provide deeper insights into structure-property relationships in this nanostructured semiconductor system.

We can get the value of Eg by use the Tauc relation , which is given by equation [17]:

$$\alpha hv = A(hv - Eg)n \qquad (2)$$

3.4. Hall effect

Tables 2 and 3 present crucial electrical and thermal properties of Cu3BiS3 (Mercaptoacetic acid) nanocomposite thin films, providing insights into their potential for various applications.

Table 2 : The table below shows the values of the Hall Effect, temperature (C), conductivity, resistivity, mobility, current, and Hall coefficient.

Temp(C)	Current[A]	Resistivity	Conductivity	Mobility	Avg. Hall
301	1.00E-08	5.23E+02	1.91E-03	1.95E+01	1.02E+04
301	1.00E-08	3.29E+02	3.04E-03	1.09E+02	3.58E+04
301	1.00E-08	1.64E+05	6.09E-06	9.55E-01	-1.57E+05

Table 2 reveals significant variations in Hall mobility, conductivity, and resistivity across three measurements at 301°C. The Hall mobility ranges from 1.02x104 to -1.57x105, indicating both positive and negative charge carriers contribute to conduction. Conductivity varies by three orders of magnitude (6.09x10-6 to 3.04x10-3), suggesting in homogeneities in the film or sensitivity to measurement conditions. The resistivity inversely correlates with conductivity, spanning from 329 to 1.64x105 units.

The electron mobility is defined by the equation [18]:

$$\upsilon d = \mu h\, E \qquad (3)$$

Table 3:table below shows data of plot of ln(σdc) versus 1000/T

Temperature(k)	Conductivity(σ)	1000/T	Ln(σ)
301	0.00191	3.32226	-6.25924
301	0.00304	3.32226	-5.79665
301	6.0937E-6	3.32226	-12.00826

Table 3 displays the relationship between electrical conductivity and temperature, which is crucial for understanding the material's thermal activation behavior. The ln(σdc) versus 1000/T plot allows for the extraction of activation energy, providing insight into the dominant conduction mechanisms. The consistent 1000/T value (3.32226) corresponds to 301K, aligning with Table 2's temperature data. These results highlight the complex electronic structure of Cu3BiS3 nanocomposites and underscore the need for further investigation into factors influencing their electrical properties, such as grain boundaries, defects, and the role

of the Mercaptoacetic acid capping agent. Understanding these properties is essential for optimizing the material's performance in potential applications like thermoelectric or optoelectronic devices.

3.5.Photovoltaic Characteristics: Dark and Illuminated I-V Curves of Cu3BiS3 Nanocomposite Solar Cells.

Figure 5 represents the I-V features of a photovoltaic cell based on Cu3BiS3 nanocomposite capped with Mercaptoacetic acid. The image includes two panels (a, b) presenting the device's performance under dark and illuminated conditions, which has wider implications for PV properties.

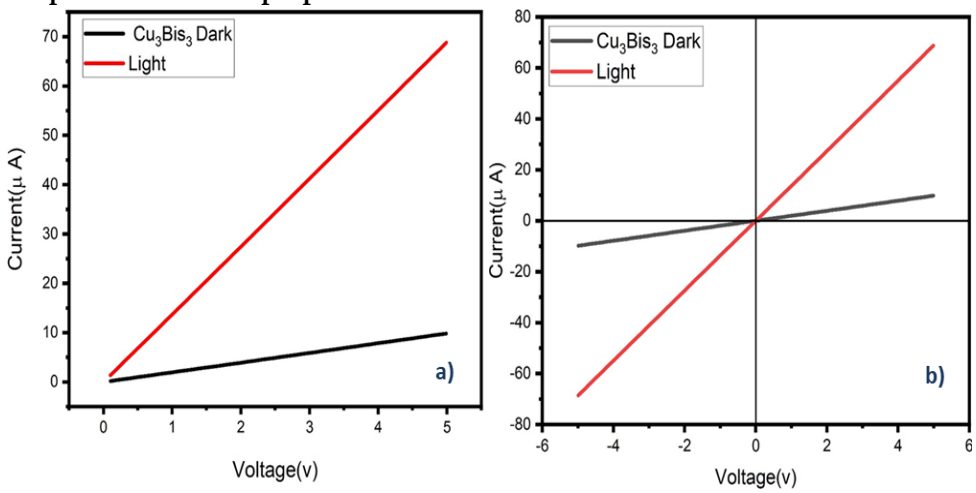

Figure 5. Typical current-voltage (I-V) characteristics for dark and light current in a solar cell of Cu3BiS3 (Mercaptoacetic acid) nanocomposite

Panel a shows the I-V curves in the first quadrant from 0 to 5 volts forward bias. The relationship between the dark current and applied voltage is a nonlinear rise as shown (dark light line) expected in a solar cell that exhibits diode-like behaviour. This curve suggests that this device has a relatively low current flow under dark conditions and can have good rectification properties. The light current line is an order of magnitude higher than the dark current, indicative of the photovoltaic effect. The linear nature of the light current curve in this voltage range signifies that the gadget operates predominantly in its series resistance-restricted region under illumination. The substantial difference between dark and light currents demonstrates the device's ability to generate photocurrent, a fundamental requirement for solar cell functionality. Plot b expands the voltage range to include both forward and reverse bias conditions (-6V to +6V), providing a more comprehensive view of the device characteristics. In the dark condition, the curve exhibits asymmetric behavior typical of a diode, with minimal current flow in reverse bias and increasing current in forward bias. This asymmetry confirms the formation of a functional p-n junction or Schottky barrier within the device structure. Under illumination, the I-V curve shifts dramatically, intersecting both the current and voltage axes. This shift is the hallmark of photovoltaic energy conversion. The key parameters that can be extracted from this curve include:1. Short-circuit current (Isc): The current at zero applied voltage, approximately 60 μA in this case , 2. Open-circuit voltage (Voc): The voltage at zero current, roughly 1.5V for this device , and 3. Fill factor: While not directly measurable from the graph, it can be calculated from the maximum power point relative to the product of Isc and Voc.The observed photovoltaic response of the Cu3BiS3 nanocomposite solar cell has several implications: 1- The significant photocurrent generation confirms the material's ability to efficiently absorb light and separate charge carriers, corroborating the favorable optical properties observed in the bandgap analysis , 2- The relatively high open-circuit voltage (~ 1.5V) aligns with the wider bandgap observed in the nanostructured material compared to its bulk counterpart, potentially leading to improved voltage output , 3- The shape of the illuminated I-V curve suggests a moderate series resistance, which could be addressed through optimization of device architecture and contact engineering to improve overall efficiency , and 4- The clear rectifying behavior in the dark

and the strong photoresponse indicate that the nanocomposite forms a good quality junction, essential for efficient charge separation and collection. To further enhance the performance of this Cu3BiS3 nanocomposite solar cell, several avenues could be explored: Optimizing the

nanocomposite morphology to enhance light trapping and charge transport , Investigating suitable buffer layers and contact materials to reduce interface recombination and improve charge extraction , Exploring the effects of various capping agents on the optoelectronic properties of the nanocomposite , and Conducting stability studies to assess the long-term performance and degradation mechanisms of the device. In conclusion, the I-V characteristics demonstrate that the Cu3BiS3 nanocomposite synthesized with Mercaptoacetic acid shows promising photovoltaic properties. The material's ability to generate significant photocurrent, coupled with its favorable bandgap, positions it as a potential candidate for next-generation solar cell applications. Further optimization of material properties and device architecture could lead to improved efficiency and practical viability of Cu3BiS3 nanocomposite-based photovoltaic devices.

3.6. Dynamic NO2 Sensing Performance of Cu3BiS3 Nanocomposites at Various Operating Temperatures.

Figure 6 presents a series of dynamic sensor response curves for a Cu3BiS3 nanocomposite-based gas sensor exposed to 30 ppm of nitrogen dioxide (NO2) at three different operating temperatures: room temperature (RT), 100°C, and 200°C.

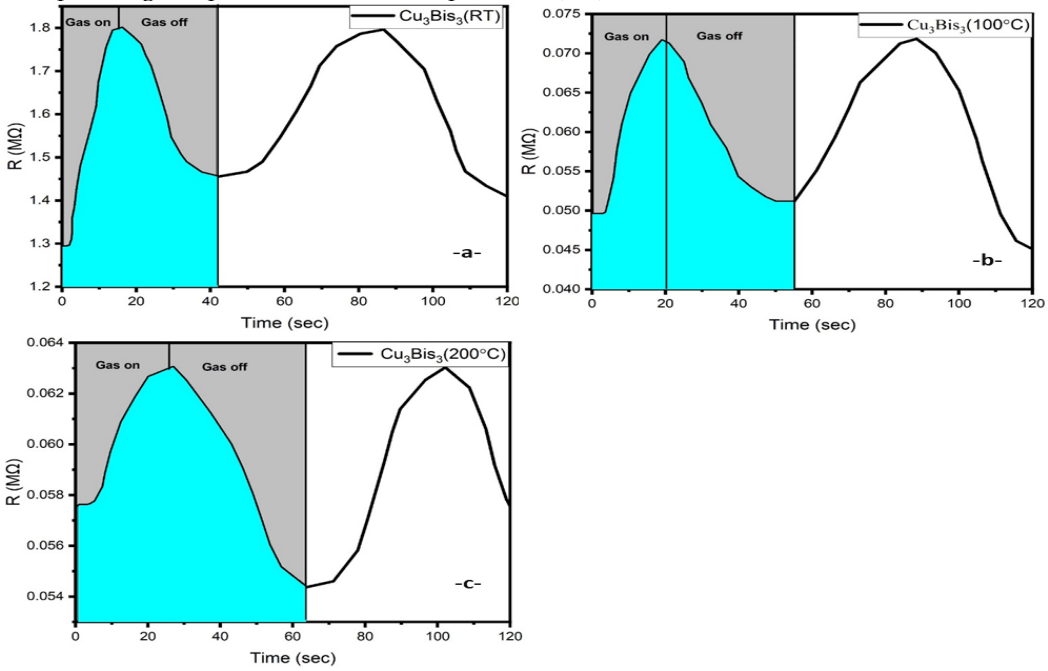

Figure 6. The repeatability dynamic sensor response curves of the sensor to 30 ppm NO2 with variations in resistance VS, time at : -a- / (RT) , -b- / (100˚C) , -c- / (200˚C) , for Cu3BiS3 (Mercaptoacetic acid) nanocomposite.

These graphs provide valuable insights into the sensing performance and temperature-dependent behavior of the nanocomposite material. Each plot displays the resistance (R) of the sensor as a function of time, with clear demarcations of gas exposure periods ("Gas on") and recovery periods ("Gas off"). The cyclic nature of these curves demonstrates the repeatability of the sensor's response, a crucial factor for practical applications.

At room temperature (Figure 5a), the sensor exhibits a significant increase in resistance upon exposure to NO2, with the peak resistance reaching approximately 1.8 MΩ. This behavior is consistent with the nature of NO2as an oxidizing gas interacting with an n-type semiconductor, where electron withdrawal from the material leads to an increase in

resistance. The response time appears relatively quick, but the recovery is notably slower, with the resistance not fully returning to the baseline within the given "Gas off" period.

At 100°C (Figure 5b), the overall resistance of the sensor decreases substantially compared to room temperature, with peak values around 0.075 MΩ. This reduction in baseline resistance is expected due to the thermal activation of charge carriers in semiconductors. The sensor maintains its responsiveness to NO2, showing a clear increase in resistance during gas exposure. Interestingly, both the response and recovery appear faster at this elevated temperature, likely due to enhanced reaction kinetics and desorption rates.

At 200°C (Figure 5c), the sensor's baseline resistance further decreases to approximately 0.064 MΩ. The response magnitude to NO2 appears somewhat reduced compared to lower temperatures, but the sensor still demonstrates clear and repeatable reactions to gas exposure. The most notable improvement at this temperature is the significantly faster recovery time, with the resistance returning close to the baseline value within the "Gas off" period.

Several key observations and implications can be drawn from these results, (1) Temperature dependence: The sensor's baseline resistance decreases with increasing temperature, following typical semiconductor behavior. This underscores the importance of temperature control in practical sensor applications. (2) Sensitivity-stability trade-off: While the room temperature sensor shows the highest relative change in resistance (sensitivity), it also exhibits the poorest recovery. Higher temperatures improve recovery times but may slightly reduce sensitivity , (3) Optimal operating temperature: Based on these results, an operating temperature around 100-200°C might offer the best compromise between sensitivity and recovery time for this Cu3BiS3 nanocomposite sensor , (4) Response mechanism: The consistent increase in resistance upon NO2 exposure across all temperatures suggests a stable sensing mechanism, likely involving electron withdrawal from the nanocomposite surface by adsorbed NO2 molecules , (5) Repeatability: The consistent response patterns across multiple cycles at each temperature demonstrate good repeatability, a crucial factor for reliable gas sensing , (6) Potential for room temperature sensing: The strong response at room temperature is particularly noteworthy, as it suggests potential for low-power sensing applications where heating is not feasible or desirable. Anyhow, a further optimization of the Cu3BiS3 nanocomposite as gas sensor towards NO2 sensing can be developed along several paths:

1. Optimizing the operating temperature for a trade-off between sensitivity and recovery time.
2. The influences of nanocomposite morphology and surface functionalization on sensing performance.
3. Discussion in terms of the different gases interfering with the sensor towards NO2.
4. Investigations into the stability over time and potential drift in sensor response within extended durations

The Mercaptoacetic acid used Cu3BiS3 nanocomposite as NO2 gas sensing material reveal promising features in terms of spanning temperatures. Recently, its room-temperature dielectric performance as well as the outstanding high-temperature sensing makes this material a flexible candidate for different gas sensing usage scenarios with specific NO2 detection requirements.

3.7.Optimizing Sensor Metrics: Response Time, Recovery Time, and Sensitivity of Cu3BiS3 Nanocomposites.

Cu3BiS3 Nanocomposite sensor synthesized by using MAA as capping agent at different temperatures is summed up in conescitive plots presented in Figure 7 and the detailed characteristics performance analysis results for Temperature Dependence obtained from.(table 5 . Table5 The primary parameters that are crucial to the study: (i) response time, (ii) recovery time, and variation in sensitivity level of Cu3BiS3 measured for the range of NO2 from 30 ppm at RT-200°C. As shown in Graph A, the response time linearly increases from 24.21 seconds at RT to 35.01 seconds at 200°C implying that the higher temperatures deteriorate the sensor's ability to rapid NO2 detection. This phenomenon might be due to

higher molecular thermal motion at high temperatures may deter NO2 molecules from adsorbing effectively on the surface of the sensor which is one of the factors that contributing into this calibration error.Recovery time (Graph B) exhibits a similar upward trend, increasing from 12.51 seconds at RT to 19.71 seconds at 200°C.

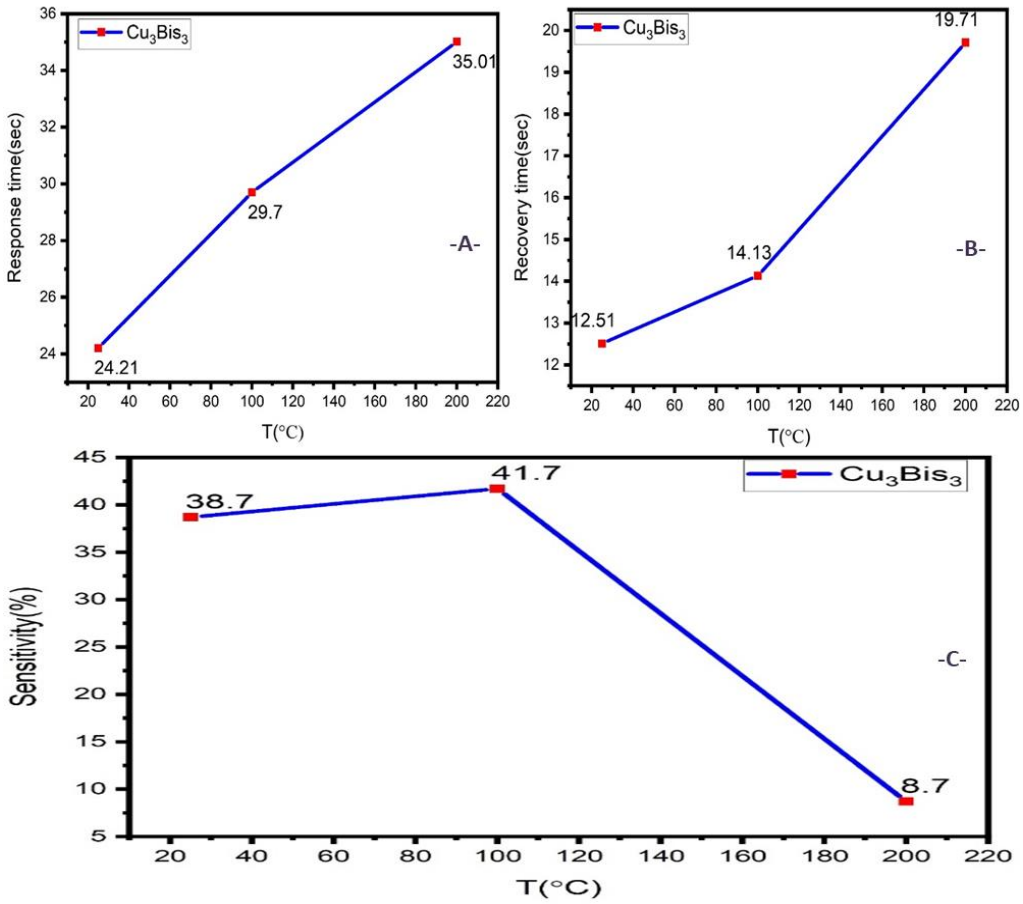

Figure 7. show the variations in –A- Recovery time operating temperatures , -B- show the variations in Response time operating temperatures , -C- show the variations in sensitivity operating temperatures , for Cu3BiS3 (Mercaptoacetic acid) nanocomposite.

However, the relationship appears non-linear, with a more pronounced increase between 100°C and 200°C. This non-linearity could indicate a threshold temperature beyond which desorption processes are significantly hindered, possibly due to stronger binding interactions or structural changes in the nanocomposite at higher temperatures. Sensitivity (Graph C) displays intriguing non-monotonic behavior. It rises slightly from 38.7% at RT to a peak of 41.7% at 100°C, before sharply declining to 8.7% at 200°C. This pattern suggests an optimal operating temperature around 100°C for maximum sensitivity. The initial increase could be due to enhanced reaction kinetics and improved charge transfer at moderate temperatures. The recovery time are, respectively from equation [19]:

Sres=(R1-R2)/R2 (4)

Table 4. The sensitivity, Response, and recovery times of the thin film sensors upon exposure to the targeting gas at different operating temperatures of Cu3BiS3 (Mercaptoacetic acid) nanocomposite

Sample	Gas type	T(⁰C)	S(%)	Response time ts(s)	Recovery time Tc(s)
Cu_3Bis_3	No_2 (30 ppm)	RT	38.7	24.21	12.51
		100	41..7	29.7	14.13
		200	8.7	35.01	19.71

The subsequent sharp decrease at higher temperatures might be attributed to thermal degradation of the nanocomposite structure, desorption of the MAA capping agent, or alterations in the material's electronic properties that adversely affect its sensing capabilities. Table 2 strengthens the findings giving exact numerical values at RT, 100°C, 200°C for sensitivity, response time, and recovery time. In the following table, one can observe the variation of these parameters against temperature changes. These show that there is a more complex temperature dependent behavior for Cu3BiS3-MAA nanocomposite sensor. Generally, as the temperatures increase, the response and recovery times decrease; however, there is a specific range of temperatures for best sensitivity. Therefore, in order to cope with these aspects of performance sensors are required at any given time to have their operating temperatures correctly regulated. This discovery indicates that more investigations are necessary for establishing unrestricted.

5. Conclusion

The Cu3BiS3 (Mercaptoacetic acid) nanocomposite synthesized in this study exhibits promising characteristics for diverse applications. Structural analysis confirms the successful formation of crystalline nanostructures with controlled morphology, while optical measurements reveal a bandgap suitable for optoelectronic devices. The material's photovoltaic response and electrical transport properties, as determined by I-V characteristics and Hall Effect measurements, indicate potential for solar cell applications. The nanocomposite's gas sensing performance, particularly towards NO2 , demonstrates a complex temperature dependence. The observed trade-offs between sensitivity, response time, and recovery time highlight the importance of optimizing operating conditions for specific sensing applications. The peak sensitivity at 100°C suggests an ideal temperature range for NO2 detection, although the decline in performance at higher temperatures warrants further investigation into thermal stability and long-term reliability. These findings contribute to the growing body of knowledge on ternary chalcogenide nanocomposites and their multifunctional capabilities. The study underscores the versatility of Cu3BiS3 nanocomposites, showcasing their potential in both energy harvesting and environmental monitoring. Future research directions may include exploring doping strategies to enhance electrical properties, investigating the sensing mechanism at the molecular level, and developing prototype devices to evaluate real-world performance.

REFERENCES

[1] Y. Khan, H. Sadia, S.Z. Ali Shah, M.N. Khan, A.A. Shah, N. Ullah, M.F. Ullah, H. Bibi, O.T. Bafakeeh, N. Ben Khedher, S.M. Eldin, B.M. Fadhl, M.I. Khan, Classification, Synthetic, and Characterization Approaches to Nanoparticles, and Their Applications in Various Fields of Nanotechnology: A Review, Catalysts. 12 (2022). https://doi.org/10.3390/catal12111386.

[2] Y. Yang, C. Liu, Y. Wang, J. Hao, Nanorods Assembled Hierarchical Bi2S3 for Highly Sensitive Detection of Trace NO2 at Room Temperature, Chemosensors. 12 (2024). https://doi.org/10.3390/chemosensors12010008.

[3] P.Shankar, J. Bosco, B. Rayappan , Gas sensing mechanism of metal oxides: The role of ambient atmosphere, type of semiconductor and gases - A review, Sci. Lett. J.4, 126 (2015).

[4] G. Kunakova, R. Meija, I. Bite, J. Prikulis, J. Kosmaca, J. Varghese, J.D. Holmes, D. Erts, Sensing properties of assembled Bi2S3 nanowire arrays, Phys. Scr. 90 (2015). https://doi.org/10.1088/0031-8949/90/9/094017.

[5] T.Wang et-al , Bifunctional gas sensor based on Bi2S3/SnS2 heterostructures with improved selectivity through visible light modulation . j.Materials Chemistry A, Issue 8 , 28 February (2022). DOI: 10.1039/D1TA10461F.

[6] J. Fonollosa, A. Solórzano, S. Marco, Chemical sensor systems and associated algorithms for fire detection: A review, Sensors (Switzerland). 18 (2018). https://doi.org/10.3390/s18020553.

[7] Rath-et-al , Solution-Processable Cu3BiS3 Thin Films: Growth Process Insightsand Increased Charge Generation Properties by Interface. ACS Appl. Mater. Interfaces 2023, 15, 41624−41633. https://doi.org/10.1021/acsami.3c10297.

[8] W.Wei et - al , Enhanced Thermoelectric Properties of Hydrothermal Synthesized BiCl3/Bi2S3 Composites. Journal of Inorganic Materials , Vol. 34 No. 3 (2019). DOI: 10.15541/jim20180261.

[9] A. Hosen, M.S. Mian, S.R. Al Ahmed, Simulating the performance of a highly efficient CuBi2O4-based thin-film solar cell, SN Appl. Sci. 3 (2021). https://doi.org/10.1007/s42452-021-04554-z.

[10] T. Varghese, C. Dun, N. Kempf, M. Saeidi-Javash, C. Karthik, J. Richardson, C. Hollar, D. Estrada, Y. Zhang, Flexible Thermoelectric Devices of Ultrahigh Power Factor by Scalable Printing and Interface Engineering, Adv. Funct. Mater. 30 (2020) 1905796. https://doi.org/10.1002/adfm.201905796.

[11] A.P. Gonçalves, E.B. Lopes, J. Monnier, J. Bourgon, J.B. Vaney, A. Piarristeguy, A. Pradel, B. Lenoir, G. Delaizir, M.F.C. Pereira, E. Alleno, C. Godart, Fast and scalable preparation of tetrahedrite for thermoelectrics via glass crystallization, J. Alloys Compd. 664 (2016) 209–217. https://doi.org/10.1016/j.jallcom.2015.12.213.

[12] Y. Zhao, X. Zhu, Y. Huang, S. Wang, J. Yang, Y. Xie, Synthesis, growth mechanism, and work function at highly oriented {001} surfaces of bismuth sulfide microbelts, J. Phys. Chem. C. 111 (2007) 12145–12148.

[13] P. Song, Y. Yang, F. Li, H. Yu, X. Dong, T. Wang, Rapid and highly sensitive detection of formaldehyde gas via a polyoxometalate–CuBi 2 O 4 composite gas sensor , Polyoxometalates. 3 (2024) 9140053. https://doi.org/10.26599/pom.2024.9140053.

[14] Tarek S. Jamil et- al , The synthesis of nano-sized undoped, Bi doped and Bi, Cu co doped SrTiO3 using two solegel methods to enhance the photocatalytic performance for the degradation of dibutyl phthalate under visible light. C. R. Chimie 20 (2017) 97-106 .http://dx.doi.org/10.1016/j.crci.2016.05.022.

[15] Y. Jian et-al , Gas Sensors Based on Chemi-Resistive Hybrid Functional Nanomaterials Nano-Micro Lett. (2020) 12:71 . https://doi.org/10.1007/s40820-020-0407-5

[16] Mohanad Q. Kareem, M.M. Ameen, S.A. Hassan, S.M. Shareef., Synthesis of Tetrahedrite Zincian Nanocomposites via solvothermal process at low temperature, 20 (2024) 40005–40013. https://doi.org/10.1016/j.ceramint.2024.07.385. University of Kirkuk.

[17] M.Q. Kareem, N.K. Hassan, Evaluation of Williamson–Hall strain and Electrical properties in WO3@ NaDCC/ITO nanoparticles thin films prepared by Hydrothermal method,IJRTEM , 3(6) 16-26 (2019). University of Kirkuk.

[18] K.R. Khedir, Z.S. Saifaldeen, T. Demirkan, R.B. Abdulrahman, T. Karabacak, Growth of zinc oxide nanorod and nanoflower structures by facile treatment of zinc thin films in boiling de-ionized water, J. Nanosci. Nanotechnol. 17 (2017) 4842–4850. https://doi.org/10.1166/jnn.2017.13432.

[19] M.Q. Kareem, N.K. Hassan, Utilization and measurements of WO3/ITO &Novel WO3@ NaDCC/ITO thin films prepared by Hydrothermal method as a Nitride Dioxide .IJMREM , 2(8) 26-33 (2019). University of Kirkuk.